Journal of King Saud University – Science 34 (2022) 101835

Contents lists available at ScienceDirect

Journal of King Saud University – Science

journal homepage: www.sciencedirect.com

Original article

Optimization of ZnO/GO nanocomposite-loaded polylactic acid active films using response surface methodology

Liew Wen Ching [a], Farah Wahida Mohd Keesan [a], Ida Idayu Muhamad [a,b,*]

[a] Department of Bioprocess and Polymer Engineering, Faculty of Engineering, Universiti Teknologi Malaysia, 81310 Johor Bahru, Johor, Malaysia
[b] IJN-UTM Cardioengineering Centre, Universiti Teknologi Malaysia, 81310 Johor Bahru, Johor, Malaysia

ARTICLE INFO

Article history:
Received 5 June 2021
Revised 15 December 2021
Accepted 12 January 2022
Available online 20 January 2022

Keywords:
PLA
ZnO nanoparticle
GO nanoparticle
Antibacterial
Active film
RSM

ABSTRACT

Development of biodegradable polymer as food packaging has been emerged with the increasing awareness of achieving sustainable development goals. As a replacement of petroleum-based polymers, Polylactic acid (PLA) has been widely utilized for food packaging. However, the main disadvantage of PLA for food packaging is its brittleness and low stiffness. Therefore, this work aimed to evaluate the potential usability of Zinc oxide (ZnO) and Graphene oxide (GO) as mechanical strengthening nanocomposites and their synergistic effect towards antibacterial property. The optimum formulation of PLA/ZnO/GO nanocomposite active film was determined using RSM by defining concentration of ZnO (0–1.5 wt%), concentration of GO (0–1.5 wt%) and mixing temperature (40, 50, 60 °C) as process parameters. The synergistic effect of ZnO/GO demonstrated a significant improvement in mechanical property. Both ZnO and GO exhibited significant antibacterial activity towards *E. coli* and *B. subtilis* and their synergistic antibacterial property performed the best with 0.75 wt% ZnO and 0.75 wt% GO at 50 °C. Results also revealed that ZnO was dominated in their synergistic effect for both mechanical and antibacterial properties. The optimum formulations for PLA/ZnO/GO nanocomposite active film were determined at 1.06 wt% ZnO, 1.11 wt % GO at 60 °C and 0.99 wt% ZnO, 1.28 wt% GO at 40 °C. The regression models by RSM were validated with the experimental results based on optimal formulations. In addition, SEM and FTIR investigation on two optimal films confirmed the good compatibility between ZnO, GO and PLA matrix. Taken together, optimized formula could provide useful insights for fabricating PLA-based active film and broadening their application in food packaging industry.

1. Introduction

Rapid growth of plastics consumption has exacerbated the waste contamination problem in the world. According to United States Environmental Protection Agency (EPA, 2021), plastics packaging and containers category had the most number of tonnage, estimated over 14.5 million tons in 2018. In consideration of the sustainability of environment, development of biodegradable biopolymer was driven extraordinarily to replace the petroleum-based synthetic polymers. Polylactic acid (PLA) is considered the most promising biopolymer due to its environmentally friendly production and biodegradation without creating problematic residual waste (Panaitescu et al., 2017). It is also permitted by the United States Food and Drug Administration (FDA) to be "Generally Recognized As Safe" (GRAS) for its use in food-contact materials or food packaging (Li et al., 2017). However, its poor toughness and brittleness limit its application in plastic industry that need plastic deformation under higher stress (Auras et al., 2004; Khan et al., 2016). In order to improve its versatility, different nanoparticles were reinforced to PLA in the light of the advancement of nanotechnology (Sharma et al., 2019) and the attractive intrinsic properties of nanoparticles include nanoscale dimensions, unique morphology, high surface area, mechanical strength and low density (Raquez et al., 2013).

Abbreviations: PLA, polylactic acid; ZnO, Zinc oxide; GO, graphene oxide; DF, degrees of freedom.

* Corresponding author at: Department of Bioprocess and Polymer Engineering, Faculty of Engineering, Universiti Teknologi Malaysia, 81310 Johor Bahru, Johor, Malaysia.
E-mail address: idaidayu@utm.my (I.I. Muhamad).

Peer review under responsibility of King Saud University.

Production and hosting by Elsevier

https://doi.org/10.1016/j.jksus.2022.101835
1018-3647/

One of the ideal nanofillers is graphene oxide (GO) nanosheet, a single monomolecular layer of graphite with a vast number of oxygen-containing functional groups include carbonyl, carboxyl, hydroxyl and epoxy to interact with many polar organic molecules and polymers. Addition of GO to PLA-based film or nanocomposite had significantly improved its mechanical property, thermal stability, gas permeability (Mao et al., 2019; Park et al., 2020; Xu et al., 2020) and antibacterial property for food industry application (Grande et al., 2017; Gu et al., 2019). The synergistic effect of GO with other nanoparticles such as zinc oxide (ZnO) even could further improve the performance of nanocomposites films. ZnO is a non-toxic, readily available, affordable and GRAS-listed (FDA, 2006) inorganic material that has great antibacterial activity (62.5–99%) against pathogenic microorganisms (Khatir et al., 2016; Rokbani et al., 2019; Wang et al., 2019).

Our previous study revealed the synergistic antimicrobial activity of GO/ZnO nanocomposite (Liew and Muhamad, 2019) but the compatibility between PLA and GO/ZnO was yet to investigate. Although some researchers reported that synergistic effect of GO and ZnO as nanohybrid had enhanced mechanical and antibacterial of PLA-based film (Huang et al., 2015), the comparison of synergistic and individual effect of nanoparticles was scarce. The effect of mixing temperature on their synergistic performance was not examined as well though different temperatures had been reported (Salehudin and Muhamad, 2018; Shankar et al., 2018). Therefore, this work aimed to further develop an effectual method for the fabrication of PLA-based film containing GO/ZnO nanocomposites based on our previous study using Response Surface Methodology (RSM). The synergistic and individual effect of GO/ZnO nanocomposites on mechanical property and antibacterial efficacy against Gram-negative (*Escherichia coli*) and Gram-positive (*Bacillus subtilis*) bacteria were assessed. Optimized formulation of PLA/GO/ZnO film was identified using desirability approach and validated by comparing the experimental results. The optimal samples were ultimately characterized to study the compatibility of nanocomposites with PLA chain via SEM and FTIR analysis. This information could be useful for development of PLA-based film as feasible active packaging for food packaging industry.

2. Materials and Methodology

2.1. Materials

Polylactide resin (Weight: >98%, Density: 1.25 g/cm^3) from Ingeo biopolymer, NatureWorks, US and chloroform (MW: 119.38; Density: 1.47 g/cm^3) from Qrec, Thailand were procured to produce PLA film. Acetone (MW: 58.08; Density: 0.789 g/cm^3) from HmbG Chemicals, Germany acted as dissolving solvent for ZnO dispersion (Concentration: 20 wt% in water; Average part size: $\leq$ 40 nm APS) from Sigma-Aldrich, US and powdered GO (Purity: >99%, Thickness: 1–5 nm, Lateral dimension: 5–10 μm, Average number of layer: 4–8, Surface area: 210 cm^2/g) from Platonic Nanotech, India to produce nanocomposite.

2.2. Fabrication of PLA/ZnO/GO nanocomposite film

Fabrication of PLA/ZnO/GO nanocomposite film was done according to Huang et al. (2015) and Salehudin and Muhamad (2018) with slight modification. A known concentration of GO nanoparticle (0–1.5 wt%) was dispersed into ZnO nanoparticle (0–1.5 wt%) with acetone and ultrasonicated at 40 °C for 1 h. Dissolved GO/ZnO solution was then dried in oven to get ZnO/GO nanocomposite and to be added into PLA solution. The final mixture undergone vigorous stirring for 3 h at different temperatures (40, 50, 60 °C). This was followed by casting on 19 cm × 19 cm acrylic plate and dried at room temperature for overnight. The final PLA/ZnO/GO nanocomposite film formed was conditioned in desiccator for 48 h prior to testing. The whole experiment was repeated to incorporate different concentrations (wt%) of GO and ZnO nanoparticles into PLA based film at different temperatures based on the designed formulations using RSM.

2.3. Experimental design using RSM

A three-factor, three-level Box-Behnken experimental design with 5 replicates at the center point and a set of points lying at the midpoint of each edge of multidimensional cube that defines the region of interested was designed. Box-Behnken has an advantage over other statistical analysis in term of accuracy and timesaving as it can determine the potential interactions between parameters with fewer number of experiments within known concentrations level. The processing variables (ZnO, GO, temperature) and predictive regression models were constructed for tensile strength (TS), Young's Modulus (YM), elongation at break (Eb), antibacterial rate (R) for *E. coli* and *B. subtilis* parameters. Experimental design involved 17 runs where all check points performed over the entire experimental domain to validate the chosen experimental design and polynomial equations. The response surface analysis was performed using Design Expert Version 6.0 software where 3D response surface plots were drawn. The quadratic model (Eq. (1)) was given as follow and fitted for each response analysed:

$$\gamma = \beta_0 + \beta_1 X_1 + \beta_2 X_2 + \beta_3 X_3 + \beta_{12} X_1 X_2 + \beta_{13} X_1 X_3 + \beta_{23} X_2 X_3 + \beta_{11} X_1^2 + \beta_{22} X_2^2 + \beta_{33} X_3^2 \quad (1)$$

where γ denotes estimated response; β_0 denotes intercept; β_1 to β_{33} are regression coefficients computed from the observed experimental values of X_1, X_2, X_3 denote coded levels of processing variables (ZnO, GO and temperature respectively). The statistical validity of the polynomials was established based on ANOVA provision in Design Expert software as well. Eventually, the feasibility and grid searches were performed to locate the composition of optimum formulations.

2.4. Mechanical property

The mechanical characteristics of films included TS, YM and Eb were evaluated using CT3 Texture Analyzer (AMETEK Brookfield, US) by referring the standard ASTM D 882-02. The TA-DGA fixture accessories which are specifically used for packaging and thin sheet polymer were employed. The gauge length was set to 5 cm with crosshead speed 0.5 mm/min. Films were cut into rectangular shape (7 cm × 1 cm) to perform the tests. A minimum of five specimens were recorded for each test and averages values for TS (Eq. (2)), YM (Eq. (3)) and percentage of Eb (Eq. (4)) were determined as follows (Yong et al., 2019):

$$\text{Tensile strength, TS(kPa)} = F/(x \times W) \quad (2)$$

$$\text{Young's Modulus, YM (MPa)} = (F \times L)/(\Delta L \times A) \quad (3)$$

$$\text{Elongation at Break, Eb (\%)} = \Delta L/L_0 \times 100 \quad (4)$$

where F denotes the stress for film fracture in Newton (N), x denotes film thickness (mm), W denotes the film width (mm), L is the length (mm), ΔL denotes the increased length when film break (mm), A denotes the area (mm), L_0 denotes the initial film length (mm).

2.5. Antibacterial activity

Antibacterial activity was performed using a viable colony count method (Shankar et al., 2018) with modification. Film sam-

ples were cut into discs with diameter 10 mm. Spoilage microorganisms such as *Bacillus subtilis* and *Escherichia coli* are studied because they are commonly found in raw, fresh and fermented products such as beef, fruits, vegetables, dairy products etc. Both bacteria were kindly provided by Faculty of Science, Universiti Teknologi Malaysia through the isolation from pineapple waste. A colony of spoilage microorganisms was inoculated in respective nutrient broths and incubated at desired conditions. An exact 100 μL of culture broth containing spoilage microorganisms was transferred to 20 mL nutrient broth contained approximate 6 mg film sample and incubated at 37 °C for 24 h under mild shaking (200 pm). The optical density (OD) readings at 600 nm were taken after 24 h of incubation. The cell viability of spoilage microorganisms was calculated by counting the bacterial colonies formed on the agar plates. The relationship between colony forming unit (CFU/mL) and OD were studied and plotted as standard curves for both *Escherichia coli* (R^2 = 0.9972) and *Bacillus subtilis* (R^2 = 0.9983). Hence, the CFU/mL results were interpolated based on the standard curves by multiplying the CFU/mL at respective OD with dilution factor. The pristine PLA film without ZnO and GO was taken as control. A minimum of three specimens were studied for each bacteria and average values for their antibacterial rate were calculated as Eq. (5):

$$\text{Antibacterial rate, } R(\%) = (N_0 - N)/N_0 x\, 100\% \quad (5)$$

where N_0 and N denote the average CFU/mL on control sample and AM film samples respectively after antibacterial evaluation.

2.6. Optimization and validation of models

In order to obtain active packaging with optimal properties (Y_1: TS, Y_2: YM, Y_3: Eb, Y_4: R/*E. coli*, Y_5: R/*B. subtilis*), numerical and graphical optimization of all independent values (X_1: ZnO, X_2: GO, X_3: temperature) were conducted using desirability approach within the limits of independent variables. The experimental results that achieved based on the suggested optimal concentrations were then compared with the predicted values by models to verify the adequacy of the regression models. The optimal films were then characterized to study their morphology and structure.

2.7. Microscopy characterization by SEM

Microstructure analysis of optimal films were done with scanning electron microscopy (SEM) model Hitachi TM3000 (Hitachi High-Technologies Corporation, Tokyo, Japan). The film surfaces (10mmx10mm) were mounted on aluminum sub using strips of double-faced carbon tape. The images were observed with an accelerating voltage of 5 kV and a current of 1750 mA.

2.8. Chemical structural analysis by FTIR

Structural changes of optimal films were observed through Fourier-Transform Infrared (FTIR) spectra. FTIR analysis was performed with Thermo Nicolet iS50 Spectrometer (Thermo Fisher Scientific Co., Waltham, MA, USA). Films (10mmx10mm) were mounted in sample compartment to determine FTIR spectra in the range of 400–4000 cm^{-1} over 16 scans averagely with resolution of 4 cm^{-1}.

3. Results and discussion

Incorporation of ZnO/GO nanocomposite into PLA with different nanocomposite concentrations and stirring temperature were studied based on proposed formulations. Experimental mean values of processing variables were elucidated in Table 1 to evaluate their effects on mechanical and antibacterial properties. Based on the results inputted into Design Expert software, the fit summary output revealed that 2FI and quadratic models were statistically significant as a function of TS, YM, Eb parameters and R. Table 2 summarized the regression coefficient and ANOVA analysis for TS, YM, Eb, R for *E. coli* and *B. subtilis*.

3.1. Effect on tensile strength

Mechanical property is one of the crucial parameters evaluating the ability of film to maintain packaging integrity against external stress and tensile factors. Table 1 showed that pristine PLA film exhibited 19.287 kPa, 0.6795 MPa and 2.99% for TS, YM and Eb respectively. Maximum TS (27.825 kPa) was obtained at 0.75 wt% ZnO and 40 °C without GO whilst minimum TS (9.051 kPa) was achieved at 1.5 wt% ZnO and 0.75 wt% GO at 40 °C. Increasing ZnO and GO concentration could improve the TS of PLA film in which its crystallinity has enhanced due to their strong interfacial interactions between nanocomposite and PLA, counteracting the brittleness of PLA matrix. Well dispersion of nanocomposites within the PLA matrix could enhance the functional groups' bonding within as well. However, overloaded ZnO and GO caused adverse effect for TS, probably due to the agglomeration of nanoparticles (Heydari-Majd et al., 2019) with the effect of temperature. Their synergistic effect was also altered by low temperature (40 °C) in this study. To maintain their high effectiveness, concentration of both ZnO and GO had to be higher than 0.75 wt % and stirred at high temperature (60 °C).

The Model F-value of 26.21 implied that this model was significant and only 0.02% chance that a "Model F-value" this large could occur due to noise, showing that it was a well-fitted model. In this case, the ZnO (X_1), GO (X_2) and interaction of ZnO (X_1) with temperature (X_3) designated as X_1 X_3 were significant model terms and ranked decreasingly as follow: $X_1 > X_1X_3 > X_2$. Insignificant lack of fit proved that this model was desirably fitted and adequately to explain the data with high coefficient of determination (R^2 = 0.9574). Ratio of adequate precision that was greater than 4 indicated adequate model discrimination. The final empirical model in term of the TS for all factors was presented as follow:

$$\gamma = 34.597 - 37.816ZnO + 6.638GO - 0.311Temp - 1.74ZnO^{*}GO + 0.644ZnO^{*}Temp - 0.061GO^{*}Temp$$

The 3D response surface for TS at fixed middle temperature (50 °C) as illustrated in Fig. 1(a) had a linear profile. It was suggested that high concentration of ZnO could negatively affect the TS which was inversely proportional to GO. Compared to GO, high concentration ZnO could agglomerate easily thereby restricting the uniform dispersion. Agglomeration, non-uniform dispersion and recrystallization of ZnO caused discontinuous cracks in PLA matrix that lowered its TS (Ngo et al., 2018). However, the limitation of ZnO could be overcome with the addition of GO. When GO was modified by the ZnO nanoparticles, more physical or chemical cross-linking points were formed to provide more favorable intermolecular interactions with PLA matrix. Perturbation plot in Fig. 1 (b) demonstrated that ZnO deviated drastically when its concentration increased, implying its significant effect. In contrast, GO and temperature did not deviate much from reference point. It was concluded that TS was positively affected by GO but negatively affected by ZnO.

3.2. Effect on Young's Modulus

Reinforcement of ZnO and GO had greatly improved the YM where the maximum response for YM (1.7783 MPa) was obtained at 0.75 wt% ZnO and 0.75 wt% GO at 50 °C. Even the minimum

Table 1
Box-Behnken design matrix used for the evaluation of the effects of processing variables on several responses.

Runs	Independent Factors			Responses					
	X_1	X_2	X_3	Y_1	Y_2	Y_3	Y_4		Y_5	
	ZnO (wt%)	GO (wt %)	Temp (°C)	Tensile Strength (kPa)	Young's Modulus (MPa)	Elongation at Break (%)	Antibacterial rate for *E. coli* (%)	Log Reduction (CFU/mL) for *E. coli*	Antibacterial rate for *B. subtilis* (%)	Log Reduction (CFU/mL) for *B. subtilis*
1	0.75	0.75	50.00	16.846	1.6805	1.03	93.52	1.167	73.18	0.571
2	1.50	0.75	40.00	9.051	1.6659	0.52	64.00	0.441	75.99	0.620
3	0.75	1.50	40.00	18.701	1.5755	1.21	58.32	0.378	87.25	0.894
4	0.00	0.75	60.00	18.401	0.6984	2.70	48.00	0.283	53.48	0.332
5	0.75	0.75	50.00	15.390	1.6064	0.99	85.52	0.830	67.55	0.489
6	0.75	0.75	50.00	15.400	1.7366	0.90	72.72	0.560	81.62	0.736
7	0.00	0.75	40.00	25.524	0.5431	4.70	16.00	0.075	45.03	0.260
8	0.75	0.75	50.00	17.457	1.5273	1.24	82.32	0.745	87.25	0.894
9	0.75	1.50	60.00	20.331	1.7196	1.21	77.52	0.643	81.62	0.736
10	0.75	0.00	60.00	16.588	1.5552	1.10	69.52	0.512	19.70	0.095
11	1.50	1.50	50.00	11.349	1.5240	0.74	64.00	0.441	59.11	0.388
12	0.75	0.00	40.00	27.825	1.1761	2.37	74.32	0.586	75.99	0.620
13	1.50	0.00	50.00	11.081	2.0362	0.56	32.00	0.167	14.07	0.066
14	0.00	0.00	50.00	19.287	0.6796	2.99	0.00	0.000	0.00	0.000
15	1.50	0.75	60.00	24.436	0.9559	2.57	75.92	0.614	81.62	0.736
16	0.00	1.50	50.00	23.471	1.1847	1.99	80.00	0.693	11.26	0.052
17	0.75	0.75	50.00	16.138	1.7783	0.97	64.72	0.450	75.99	0.620

Table 2
Regression coefficient and ANOVA analysis for tensile strength, Young's Modulus, elongation at break and antibacterial rate for *E. coli* and *B. subtilis*.

Coefficient Estimate		Y1: Tensile Strength (kPa)		Y2: Young's Modulus (MPa)		Y3: Elongation at Break (%)		Y4: Antibacterial rate for *E. coli* (%)		Y5: Antibacterial rate for *B. subtilis* (%)	
			Prob > F		*Prob > F*		*Prob > F*		*Prob > F*		*Prob > F*
Model F-value		26.21	0.0002*	[a]29.75	0.0026*	113.46	0.0002*	8.13*	0.0294*	23.37	0.0041*
Sum of squares											
Model		195.74	(DF: 6)	2.72	(DF: 9)	16.94	(DF: 9)	9232.08	(DF: 9)	12161.52	(DF: 9)
Residual		8.71	(DF: 7)								
Lack of Fit		5.43[a]	(DF: 3)								
Pure Error		3.29	(DF: 4)	0.041	(DF: 4)	0.066	(DF: 4)	504.83	(DF: 4)	231.32	(DF: 4)
Cor Total		204.45	(DF: 13)	2.76	(DF: 13)	17.00	(DF: 13)	9736.91	(DF: 13)	12392.85	(DF: 13)
Standard Deviation		1.12		0.10		0.13		11.23		7.60	
Mean		17.57		1.42		1.59		60.30		54.68	
R^2		0.9574		0.9853		0.9961		0.9482		0.9813	
Adjusted R^2		0.9208		0.9522		0.9873		0.8315		0.9393	
Adequate Precision		18.589		17.533		38.071		8.426		13.576	
Regression Model		2FI		Quadratic		Quadratic		Quadratic		Quadratic	
Regression coefficient			*Prob > F*		*Prob > F*		*Prob > F*		*Prob > F*		*Prob > F*
Intercept	β_0	16.58		1.67		1.02	33.60	79.76		77.12	
Linear	β_1	−5.18	<0.0001*	0.42	0.0011*	−0.92	−19.84	4.00	0.5157	15.48	0.0152*
	β_2	1.72	0.0079*	−1.714E-003	0.9745	−0.20	−15.92	28.00	0.0076*	14.07	0.0208*
	β_3	1.27	0.1352	−0.012	0.8986	−0.26	−23.92	33.60	0.0260*	−19.70	0.0403*
Quadratic	β_{11}			−0.46	0.0029*	0.96	−12.00	−19.84	0.0647	−30.82	0.0044*
	β_{22}			0.15	0.1042	−0.41	17.60	−15.92	0.1123	−25.19	0.0090*
	β_{33}			−0.16	0.0801	0.80	−24.00	−23.92	0.0380*	18.44	0.0255*
Interactions	β_{12}	−0.98	0.1228	−0.25	0.0072*	0.30	0.0101*	−12.00	0.0995	8.44	0.0905
	β_{13}	4.83	0.0030*	−0.089	0.4713	0.74	0.0067*	17.60	0.2338	−23.92	0.0481*
	β_{23}	−0.46	0.5642	0.084	0.3908	0.26	0.0817	−24.00	0.0692	16.89	0.0624

DF: Degrees of freedom.
*Tern that was tested significant to evaluate its effect on response variables when Prob > F less than 0.05.
[a] Term that was tested not significant when P > F greater than 0.100.

response (0.5431 MPa) that achieved at 0.75 wt% GO and 40 °C without ZnO was also comparable to pristine PLA which was 0.6796 MPa. In the absence of ZnO, lower concentration of GO did not contribute much to the YM unless it was in high concentration (1.5 wt%). This was because high GO concentration provided more hydrogen bonds available for stronger bonds' interactions between GO and PLA matrix (Lagarón et al., 2016). Moreover, increase of rigidity was in good correlation with the ZnO concentration. Similar positive trend was depicted by Pantani et al. (2013) when ZnO was increased from 1 to 2 wt%. The values of YM were corresponded to the TS, implying that ZnO was dominated in the synergistic effect of ZnO and GO in mechanical property enhancement.

The Model F-value of 29.75 implied that this model was significant and good fitted. The ZnO (X_1), second order effect of ZnO (X_1^2) and interaction of ZnO (X_1) with GO (X_2) designated as X_1X_2 were significant model terms and their decreasing order was: $X_1 > X_1^2 > X_1X_2$. It was proven that temperatures had insignificant effect on the YM since most of the formulations performed similar YM values (1.1–2.0 MPa) for all temperatures. This quadratic

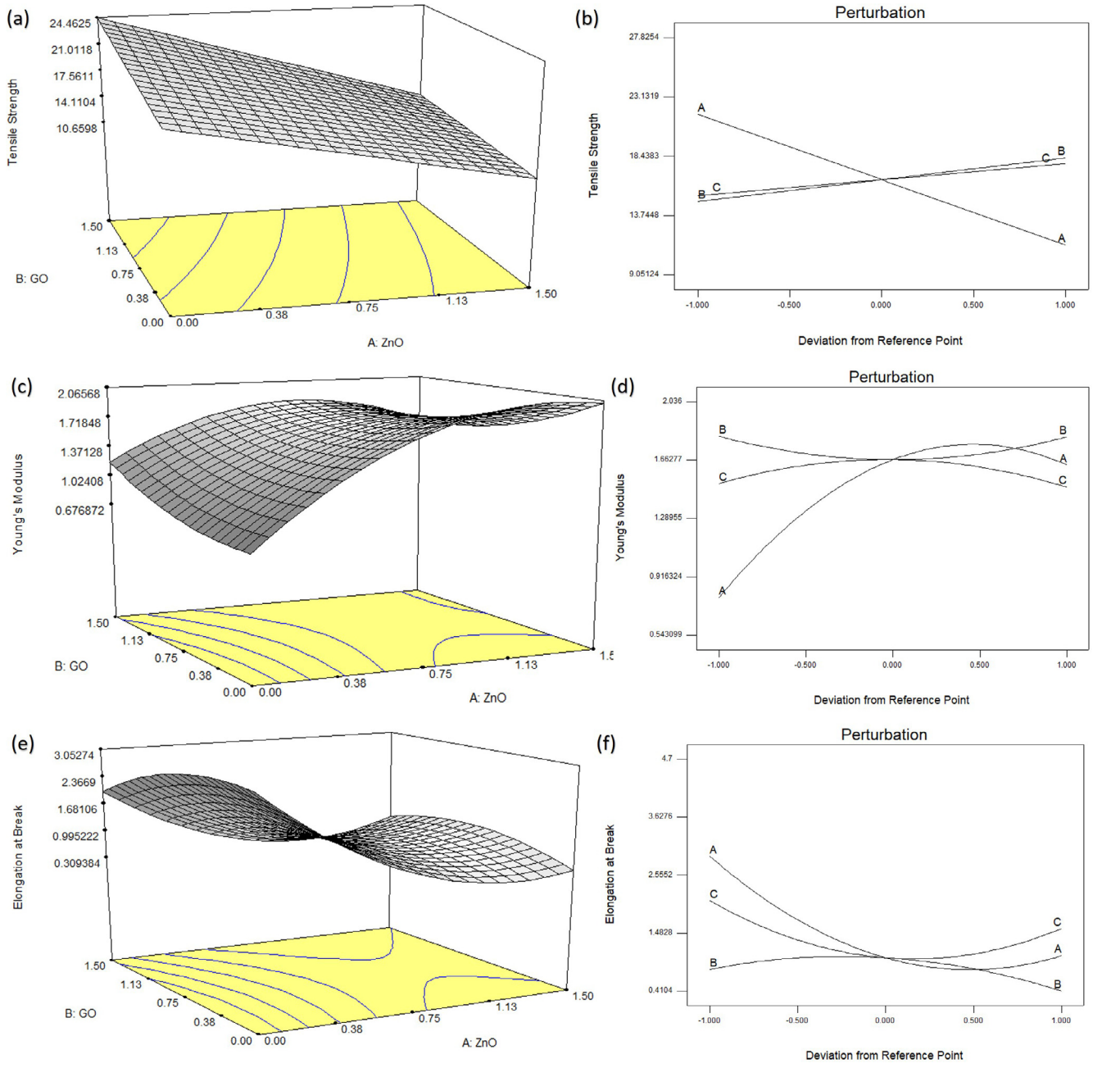

Fig. 1. 3D response surfaces for (a) Tensile strength, (c) Young's Modulus, (e) Elongation at break and Perturbation plots for (b) Tensile strength, (d) Young's Modulus, (f) Elongation at break. Linear and hyperbolic profile illustrated the changeable effect of variables on responses at fixed middle temperature (50 °C). The perturbation plots demonstrated that ZnO had significant deviation from reference point.

model was fitted and adequately to explain the data with high coefficient of determination (R^2 = 0.9853). The adequate precision value of 17.533 suggested adequate model discrimination and its final empirical model in term of the YM for all factors was presented as follow:

$$\gamma = -3.390 + 2.72ZnO - 0.616GO + 0.163Temp - 0.813ZnO^2 + 0.262GO^2 - 0.00164Temp^2 - 0.452ZnO^*GO - 0.0119ZnO^*Temp + 0.0112GO^*Temp$$

Fig. 1(c) that presented 3D response surface for YM at fixed middle temperature (50 °C) had a hyperbolic profile in accordance with the quadratic model. Generally, increasing ZnO could improve the performance of YM but it could be further enhanced with the addition of GO. However, the great performance was limited by high GO concentration. The limitation was probably due to the agglomeration of nanoparticles and percolated network effect of excessive GO and ZnO (Marques et al., 2012). Hence, higher level (1.5 wt%) of ZnO or middle level (0.75 wt%) of GO/ZnO were preferable for the greatest result. This could be further explained from the perturbation plot in Fig. 1(d) where ZnO factor deviated significantly from reference values.

3.3. Effect on elongation at break

Eb was deduced inversely proportional to TS and YM as increment of ZnO and GO concentration resulted a decrease in Eb. Table 1 showed that pristine PLA film exhibited the second highest

Eb which was 2.99%. The maximum Eb (4.7%) was achieved at 0.75 wt% GO and 40 °C without ZnO whilst minimum value (0.52%) obtained at 1.5 wt% ZnO and 0.75 wt% GO at 40 °C. The homogeneous distribution of nanocomposites in PLA matrix enhanced the interactions bonds with nanocomposite but also undergone plastic deformation with higher crystallinity and lower flexibility. The crystallinity of PLA was mainly contributed by ZnO thus the individual or synergistic effect of ZnO was more significant compared to other variables. This was in agreement with the influence order of significant terms which was ranked decreasingly as follow: $X_1 > X_1^2 > X_3^2 > X_1X_3 > X_1X_2$, $X_2^2 > X_2$ where terms were ZnO, second order effect of ZnO, second order effect of temperature, interaction of ZnO with temperature, interaction of ZnO with GO, second order effect of GO and GO. Effect of temperature on Eb was notable also since 60 °C obtained higher Eb value than 40 °C when the concentration of ZnO and GO was same. In order to improve the plasticity and reduce film resistance of PLA film, it was suggested to add in plasticizer such as glycerol or polyethylene glycol (PEG) into PLA matrix (Byun et al., 2010).

Based on the ANOVA analysis in Table 2, the Model F-value of 113.46 suggested that this quadratic model was significant and low "Model F-value" represented a well fitted model. Overall, high coefficient of determination (R^2 = 0.9961) indicated the data could be adequately explained in this model. On the other hand, adequate precision of 38.701 stating adequate model discrimination since its ratio was greater than 4. The final empirical model in term of the Eb for all factors was presented as follow:

$$\gamma = 29.218 - 9.122ZnO - 1.285GO - 0.923Temp + 1.702ZnO^2 - 0.733GO^2 + 0.00798Temp^2 + 0.526ZnO^*GO + 0.0989ZnO^*Temp + 0.0344GO^*Temp$$

The effect of different factors at fixed middle temperature (50 °C) on Eb was presented by 3D response surface in Fig. 1(e) as a hyperbolic profile. The Eb value was slightly increased with the low concentration of GO but gradually dropped at high concentration. Meanwhile, increasing ZnO decreased the response value gradually until it reached 1.13 wt% ZnO to become static. Generally known that TS that represents stress is inversely proportional to Eb which represents plasticity. Yet Eb response resembled the decreasing trend for TS in this study. The highest Eb value was achieved at low concentration of GO and without ZnO. This was probably due to the strong interface between nanocomposites and polymer matrix that restricted the movement of PLA chain (Kanmani and Rhim, 2014; Yuan et al., 2018). The deviation change of each factors was demonstrated with perturbation plot in Fig. 1(f) where ZnO factor deviated the most compared to GO and temperature factors.

3.4. Effect on antibacterial rate

The cell viability of *E. coli* and *B. subtilis* after 24 h of incubation was demonstrated in Fig. 2. Results showed that increment of both ZnO and GO concentration demonstrated a positive trend in antibacterial rate for *E. coli* especially due to their synergistic effect. As high as 93% of antibacterial rate could be achieved by the synergistic effect of ZnO and GO. Film containing GO induced friction and weakened the outer membrane of the cell causing the cell to be exposed whilst Zn^{2+} from ZnO was in contact with negatively charged bacterial membrane, resulting a protein solidification and enzyme inactivation. These occurrences were further inhibiting the growth of bacteria (Zhong et al., 2018). However, the synergistic effect of ZnO and GO was remarkably affected by temperature where lower (40 °C) and higher temperature (60 °C) performed lower antibacterial rate. These temperatures also negatively affected the performance of individual GO or ZnO when incorporated into PLA matrix. The maximum R for *E. coli* (93.52%) was determined at 0.75 wt% ZnO and 0.75 wt% GO at 50 °C. This was significantly different from the minimum rate (16%) that obtained at 0.75 wt% GO at 40 °C without ZnO. Hence, the optimum R was at the middle temperature (50 °C) with the middle level (0.75 wt%) ZnO or GO.

Based on Table 2, The Model F-value of 8.13 suggested that this quadratic model was significant and only 2.94% chance that a "Model F-value" this large could occur due to noise, proving that it was a well fitted model. The significant model terms for this case were GO (X_2), temperature (X_3), second order effect of temperature (X_3^2) and their influence was ranked decreasingly: $X_2 > X_3^2 > X_3$. In general, high coefficient of determination (R^2 = 0.9482) and high adequate precision indicated the model could be adequately explained and discriminated. The final empirical model in term of the R for *E. coli* for all factors was presented as follow:

$$\gamma = -798 - 43.09ZnO + 255.79GO + 27.92Temp - 35.28ZnO^2 - 28.30GO^2 - 0.2392Temp^2 - 21.33ZnO^*GO + 2.347ZnO^*Temp - 3.2GO^*Temp$$

Fig. 3(a) illustrated 3D response surface to evaluate the effect of different factors at fixed middle temperature (50 °C) on R for *E. coli*. The increment of both GO and ZnO improved the antibacterial rate but the performance of GO was more significant than ZnO. Superior antibacterial rate (93.52%) was achieved by the synergistic effect of GO (1.5 wt%) and ZnO (0.75 wt%). This was owing to the strong interaction of GO and ZnO with the bacterial membrane which paralyzed the proliferating capabilities of bacteria, high dispersibility and compatibility of GO with polymer matrix (Wu et al., 2020). Furthermore, the electrons transferred between ZnO and GO can absorb surface oxygen to form different reactive oxygen species (ROS) which induced lipid peroxidation and ultimately damaged the bacterial membrane (Zhong and Yun, 2015). Researchers also claimed that electrons transferred from bacterial membrane to graphene surface could cause oxidative stress through ROS-independent pathway to induce bacterial death (Cobos et al., 2020). It summarized that both GO and ZnO performed great antibacterial activity against *E. coli* at middle temperature (50 °C). The deviation change of each factors was illustrated with perturbation plot in Fig. 3(b) where temperature and GO factors deviated the most compared to ZnO factor.

Similar notable antibacterial property by their synergistic effect was observed for *B. subtilis* at all temperatures, achieving 67% to 87%. This was attributed to the synergistic effect of Zn ions to bind tightly with bacterial membrane thereby disrupting its proliferation. Special 2D structure of GO that reacted strongly with bacterial lipid bilayer could damage its membrane as well (Zhong and Yun, 2015). Meanwhile, the individual antibacterial performance of GO or ZnO was correlated to the temperature as ZnO exhibited greater antibacterial property than GO at 40 °C. On the contrary, GO had better antibacterial performance than ZnO at 60°. It was suggested that higher temperature could distort the dispersion of ZnO in PLA matrix thereby negatively influencing its performance. The maximum R for *B. subtilis* (87.25%) was determined at 0.75 wt% ZnO, 0.75 wt% GO at 50 °C and 1.5 wt% ZnO, 0.75 wt% GO at 40 °C. The minimum rate (11.26%) was obtained at 1.5 wt% GO at 50 °C without ZnO.

The quadratic model was proven significant and well fitted with large Model F-value and low Prob > F. Most of the model terms were significant, including ZnO (X_1), GO (X_2), temperature (X_3), second order effect of ZnO (X_1^2), second order effect of GO (X_2^2), second order effect of temperature (X_3^2) and interaction of ZnO (X_1) with temperature (X_3) which designated as X_1 X_3. Their order of

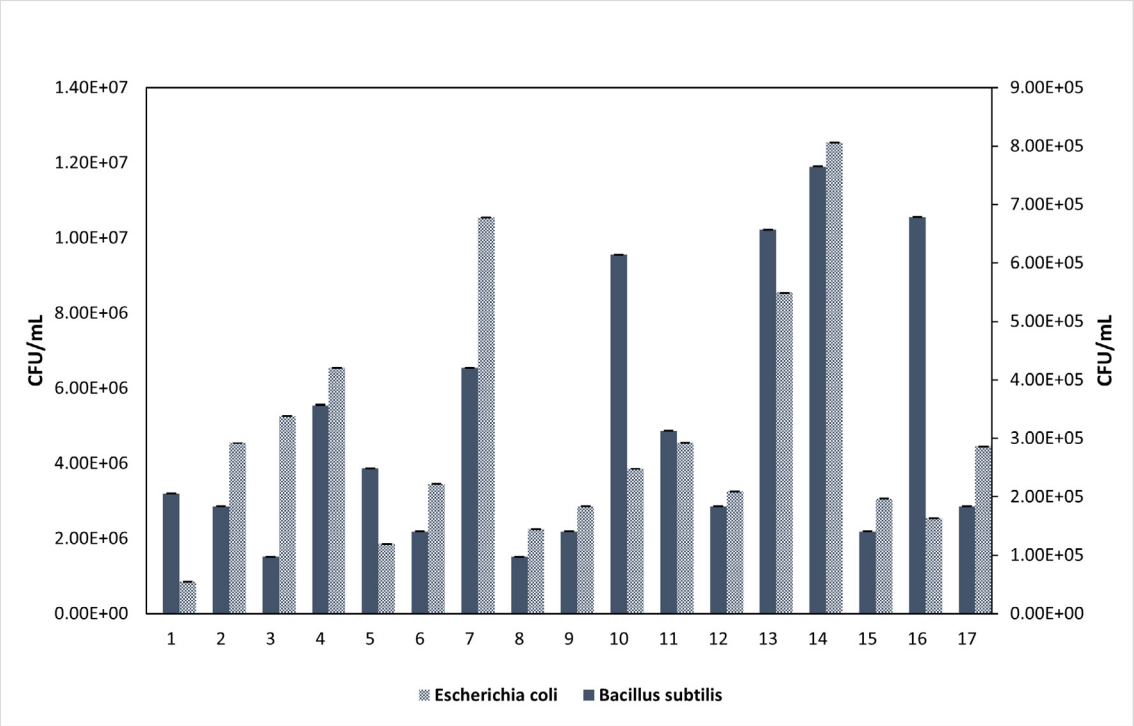

Fig. 2. Cell viability of *E. coli* and *B. subtilis* after 24 h of incubation.

influence was ranked decreasingly as follow: $X_1^2 > X_2^2 > X_1 > X_2 > X_3^2 > X_3 > X_1 X_3$. In summary, the coefficient of determination ($R^2 = 0.9813$) was high enough to indicate the data was adequately represented in this model. Adequate model discrimination was also shown from the large adequate precision. The final empirical model in term of the R for *B. subtilis* for all factors was presented as follow:

$$\gamma = 524.22 + 251.06ZnO - 37.90GO - 19.70Temp - 54.79ZnO^2 - 44.78GO^2 + 0.184Temp^2 + 15.01ZnO^*GO - 3.19ZnO^*Temp + 2.252GO^*Temp$$

The 3D response surface for effect of different factors at fixed middle temperature (50 °C) on R for *B. subtilis* evaluation was illustrated in Fig. 3(c). The hyperbolic profile of the graph depicted that increment of both GO and ZnO individually could improve the antibacterial rate yet to some extent only, approximately after 0.75 wt% concentration would cause adverse effect. It was also notable that ZnO had more significant performance than GO if compared individually. Similar to the previous discussion, the synergistic effect of ZnO and GO had the greatest performance, especially when both reached 0.75 wt%. The antibacterial rate was also affected by the concentration and composition since low concentration might be insufficient to inhibit the bacterial activity whereas stacking or well-adhesion of nanoparticles to each other at high concentration might diminish the antibacterial performance (Gouvêa et al., 2018). The deviation change of each factor was illustrated with perturbation plot in Fig. 3(d) where temperature factor deviated the most compared to ZnO and GO factor.

Both ZnO and GO showed higher susceptibility of Gram-positive, *B. subtilis* than the Gram-negative, *E. coli*. This could be related to the differences in cell wall structure where *B. subtilis* had thick peptidoglycan layer surrounded by negative charge bonds, thereby had more affinity towards the positively charge ion, Zn^{2+} compared to the *E. coli* that consisted thin peptidoglycan layer (Esmailzadeh et al., 2016). It could also be inferred that GO did not exhibit antibacterial property as great as ZnO individually and overloaded ZnO might cause uniform dispersion which further affected the antibacterial performance.

3.5. Multiple responses optimization and validation

Optimization of multiple responses using desirability approach is desired to determine the optimal food packaging film with great mechanical strength and antibacterial property. In this study, all the responses were maximized and the processing variables (ZnO, GO and temperature) were studied within their range of level. There were two comparable compromised formulations. The first formulation (PLA40) was interpolated at 0.37 wt% ZnO, 1.28 wt% GO and 40 °C with 0.611 desirability. Contrarily, the processing variables were set at 0.99 wt% ZnO, 1.10 wt% GO and 60 °C for second formulation (PLA60) with 0.601 desirability. The 3D surface responses for both desirability were illustrated in Fig. 4(a) and (b).

Based on the proposed formulations, it was noticed that the concentration of GO did not vary much (1.11–1.28 wt%) to achieve the optimum results whilst the concentration of ZnO was varied with temperature. Lower concentration of ZnO (0.37 wt%) was preferred at lower temperature (40 °C). Contrarily, higher temperature (60 °C) would accompany with higher ZnO concentration (1.06 wt %). Lower ZnO concentration could achieve better mechanical properties but lower antibacterial rate compared to the higher ZnO concentration. This inferred that ZnO was the determining factor in this formulation whereas GO was the supporting material to achieve the comparable performance of mechanical properties. Hence, it could be concluded that the ZnO concentration was adaptable based on temperature while the GO could be fixed at middle level concentration in this formulation. In consideration of the optimal antibacterial rate, PLA60 is chosen over PLA40 for its higher antibacterial rate and comparable mechanical properties with control sample.

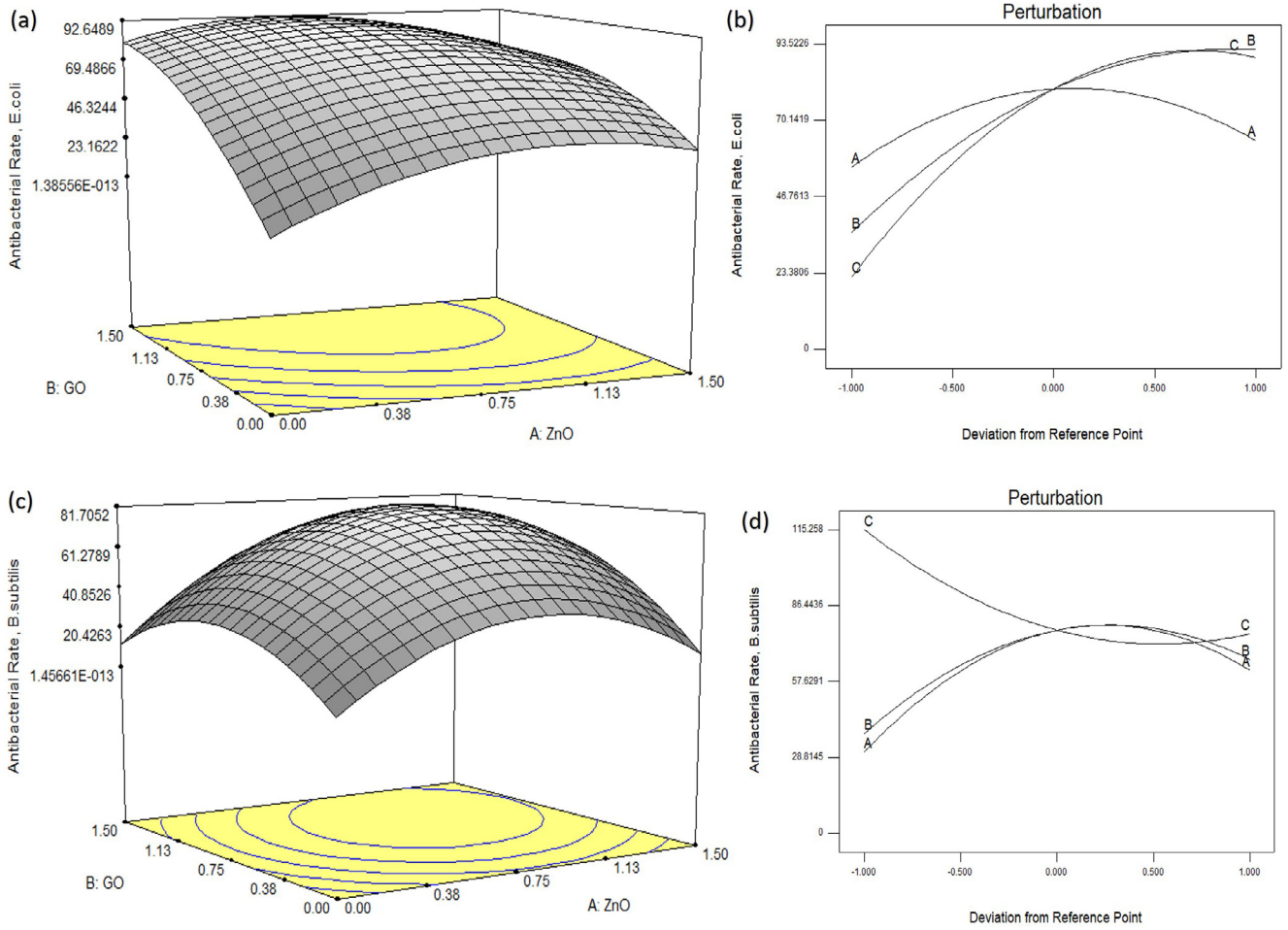

Fig. 3. 3D response surfaces for antibacterial rate against (a) *E. coli*, (c) *B. subtilis* and Perturbation plots for (b) *E. coli*, (d) *B. subtilis*. Hyperbolic profile illustrated that maximum response obtained at the middle level of ZnO/GO concentration. Temperature deviated the most from reference point in the perturbation plots.

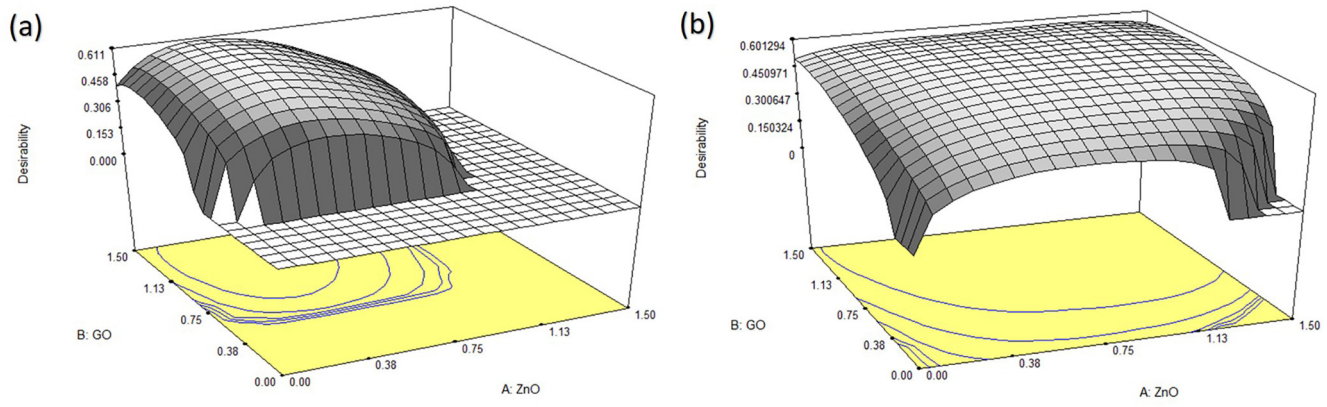

Fig. 4. 3D response surfaces for the optimization of multiple responses using desirability approach at (a) 40 °C and (b) 60 °C. Even though 40 °C had higher desirability, its value decreased drastically when ZnO and GO increased. Meanwhile, hyperbolic profile in 60 °C had comparable desirability for all level of ZnO and GO concentration.

In order to validate the adequacy of proposed models, the predicted values for responses were compared with the actual experimental values based on 2 optimum formulations. The comparison was summarized in Table 3 where their percentage errors were calculated. The results demonstrated that all actual values were acceptably close to the predicted values since all percentage errors were not more than 16%. This validated the empirical models developed from Box-Behnken software were reasonably adequate for all the responses especially for TS and R. The proposed optimum formulations were also satisfactorily employed and examined in following section.

3.6. Microstructure study of composite using SEM

The influence of ZnO/GO nanocomposite on the microstructure of PLA was investigated by SEM as illustrated in Fig. 5. The micro-

Table 3
Comparison of predicted and actual values of responses and their percentage error.

Responses	Predicted value	Actual value	Percentage error* (%)
PLA40			
TS (kPa)	22.2229	22.5749	1.5840
YM (MPa)	1.2464	1.1024	11.5533
Eb (%)	2.51058	2.2267	11.3073
R/*E. coli* (%)	57.3053	56.2220	1.8904
R/*B. subtilis* (%)	70.0245	65.8393	5.9768
PLA60			
TS (kPa)	18.1956	17.8658	1.8125
YM (MPa)	1.58397	1.3732	13.3064
Eb (%)	1.58108	1.3280	16.0068
R/*E. coli* (%)	90.8209	88.7525	2.2775
R/*B. subtilis* (%)	80.4274	78.2091	2.7581

*Percentage error = [(Actual value – Predicted value)/Predicted value] × 100%.

graph of pristine PLA showed a clean but not very smooth surface with crazes, proving the brittleness behavior and plastic deformation of PLA at high temperature. On the other hand, the flakes of ZnO/GO were evident on the surface of PLA60, showing the dispersion of ZnO/GO nanocomposite within PLA matrix. However, the flakes were bigger in size than that in PLA40 which had smaller and separated flakes. This could be attributed to the agglomeration of ZnO/GO nanocomposites when they were at high concentration. In accordance with Huang et al. (2015), this might be attributed to the distance between two ZnO/GO nanocomposite were small until they inclined to stack together. Although the GO concentration was higher in PLA40 (1.28 wt%), lower ZnO concentration in within (0.37 wt%) had counteracted the agglomeration of nanocomposites thus they were not stacked together and dispersed homogeneously in PLA matrix. These results inferred a satisfactory interaction and compatibility between PLA, ZnO and GO but the interactions could be influenced by the high concentration of nanocomposite.

3.7. Chemical interactions study using FTIR

The intermolecular interactions between PLA biopolymer chains and nanoparticles were analyzed using FTIR. As indicated by Fig. 6, FTIR of three samples presented main absorbance regions in the range of 1000–1800 cm^{-1} and 600–900 cm^{-1}. Overall, the FTIR absorbance peaks of control, PLA40 and PLA60 were similar indicating they were exhibiting the same chemical composition. Specifically, all the three samples had absorption band near 752 cm^{-1} which represented C=C bending. The characteristics of stretching vibration in ZnO nanoparticles was shown at 667 cm^{-1} in accordance with Rajaura et al. (2017) and Ubaidullah et al. (2020). The peaks around 868 cm^{-1}, 1380 cm^{-1},

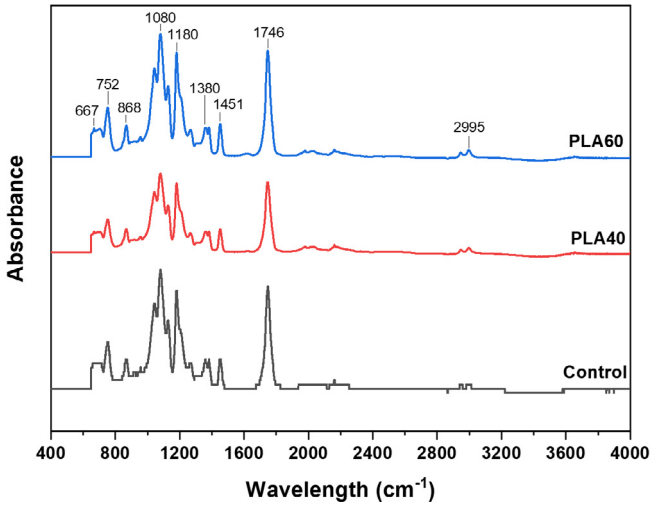

Fig. 6. FTIR spectra of control and optimal films based on optimum formulations.

1451 $cm^{-1}$and 2995 cm^{-1} were associated with the C–H stretching that contributed by the saturated hydrocarbons (Sabbagh et al., 2021; Shankar et al., 2018). The intense peaks at 1746 cm^{-1} were ascribed to the C=O stretching vibrations of ester groups in PLA molecules (Qu et al., 2010). The spectra of 1080 cm^{-1} and 1180 cm^{-1} also demonstrated the presence of C-O stretching and bending vibrations in GO and ZnO lattice (Lavand and Malghe, 2018). Apparently, as the concentration of GO increased, the absorption bands became wider and lower as shown by PLA40 which has 1.28 wt% GO. The addition of high ZnO concentration (0.99 wt%) in PLA60 did not affect the absorption bands yet the effect of higher ZnO concentration (>1 wt%) was still unknown that need further investigation. It was deduced that GO had more remarkable effect on the intermolecular interactions within PLA than ZnO in this study. In overall, the insignificant change of absorbance peaks of all samples implied that addition of GO and ZnO would not affect the chemical structure of PLA biopolymer chain. It also implied that ZnO and GO nanoparticles could work well as a promising nanocomposite to be incorporated into PLA-based biopolymer.

4. Conclusion

Box-Behnken experimental results revealed that ZnO and GO nanoparticles were incorporated successfully into PLA matrix at different temperatures. ZnO, GO and temperature could positively affect the mechanical and antibacterial properties of PLA film but

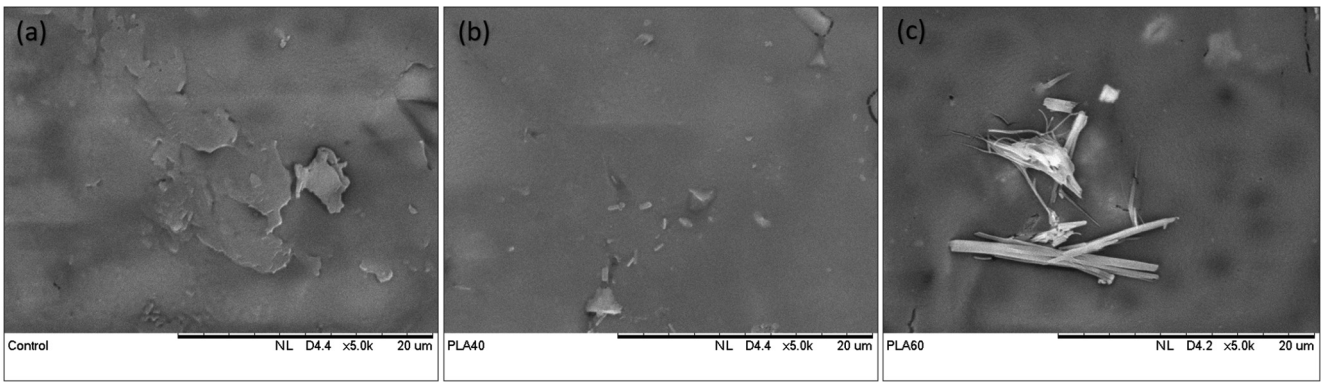

Fig. 5. SEM images at 5000× magnification for samples (a) control, (b) PLA40 and (c) PLA60.

was negatively affected by low temperature (40 °C). Both ZnO and GO exhibited significant antibacterial activity towards *E. coli* and *B. subtilis* especially their synergistic antibacterial effect. Optimum formulations were achieved at 40 °C and 60 °C using RSM. The adequacy of each model was validated by optimal formulations and proved that the models were well fitted. With optimal formulations, SEM showed that ZnO/GO nanocomposites exhibited good intercalation in PLA matrix whilst FTIR spectra indicated that nanocomposites could blend well with PLA biopolymeric chain. Overall, synergistic effect of ZnO and GO as nanocomposites could be potentially utilized for active food packaging to extend food shelf life. Further investigation on the biodegradation of film and kinetic release of nanocomposites could be done. The application of this active film could be further examined for its antibacterial effect of nanocomposites on real food monitoring as well.

Declaration of Competing Interest

The authors declare that they have no known competing financial interests or personal relationships that could have appeared to influence the work reported in this paper.

Acknowledgements

The authors would like to thank the Malaysia Ministry of Higher Education and Universiti Teknologi Malaysia for financial support through Malaysia Research University Network (MRUN) under project number R.J130000.7851.4L868. The authors would also like to extend gratitude to technicians of Dept. of Bioprocess and Polymer Engineering, Food and Biomaterial Engineering Research Group (FoBERG) and Faculty of Science from Universiti Teknologi Malaysia for their assistance in this study.

References

Auras, R., Harte, B., Selke, S., 2004. An overview of polylactides as packaging materials. Macromol. Biosci. 4 (9), 835–864. https://doi.org/10.1002/mabi.200400043.

Byun, Y., Kim, Y.T., Whiteside, S., 2010. Characterization of an antioxidant polylactic acid (PLA) film prepared with α-tocopherol, BHT and polyethylene glycol using film cast extruder. J. Food Eng. 100 (2), 239–244. https://doi.org/10.1016/j.jfoodeng.2010.04.005.

Cobos, M., De-La-Pinta, I., Quindós, G., Fernández, M.J., Fernández, M.D., 2020. Graphene oxide–silver nanoparticle nanohybrids: Synthesis, characterization, and antimicrobial properties. Nanomaterials 10 (2), 376. https://doi.org/10.3390/nano10020376.

EPA, 2021. Containers and Packaging: Product-Specific Data [WWW Document]. URL https://www.epa.gov/facts-and-figures-about-materials-waste-and-recycling/containers-and-packaging-product-specific-data.

Esmailzadeh, H., Hejazi, J., Khaksar, R., Shahraz, F., Sangpour, P., Shahraz, F., Hejazi, J., Khaksar, R., 2016. Effect of nanocomposite packaging containing ZnO on growth of Bacillus subtilis and Enterobacter aerogenes. Mater. Sci. Eng. C 58, 1058–1063. https://doi.org/10.1016/j.msec.2015.09.078.

FDA, U.S., 2006. EAFUS : A Food Additive Database. Centre for Food Safety and Applied Nutrition, U.S. Food and Drug Administration. Washington, DC, USA.

Gouvêa, R.F., Del Aguila, E.M., Paschoalin, V.M.F., Andrade, C.T., 2018. Extruded hybrids based on poly(3-hydroxybutyrate-co-3-hydroxyvalerate) and reduced graphene oxide composite for active food packaging. Food Packag. Shelf Life 16, 77–85. https://doi.org/10.1016/j.fpsl.2018.02.002.

Grande, C.D., Mangadlao, J., Fan, J., De Leon, A., Delgado-Ospina, J., Rojas, J.G., Rodrigues, D.F., Advincula, R., 2017. Chitosan cross-linked graphene oxide nanocomposite films with antimicrobial activity for application in food industry. Macromol. Symp. 374, 1–8. https://doi.org/10.1002/masy.201600114.

Gu, X., Li, Y., Cao, R., Liu, S., Fu, C., Feng, S., Yang, C., Cheng, W., Wang, Y., 2019. Novel electrospun poly(lactic acid)/poly(butylene carbonate)/graphene oxide nanofiber membranes for antibacterial applications. AIP Adv. 9 (6), 065315. https://doi.org/10.1063/1.5100109.

Heydari-Majd, M., Ghanbarzadeh, B., Shahidi-Noghabi, M., Najafi, M.A., Hosseini, M., 2019. A new active nanocomposite film based on PLA/ZnO nanoparticle/essential oils for the preservation of refrigerated Otolithes ruber fillets. Food Packag. Shelf Life 19, 94–103. https://doi.org/10.1016/j.fpsl.2018.12.002.

Huang, Y., Wang, T., Zhao, X., Wang, X., Zhou, L.u., Yang, Y., Liao, F., Ju, Y., 2015. Poly (lactic acid)/graphene oxide-ZnO nanocomposite films with good mechanical, dynamic mechanical, anti-UV and antibacterial properties. J. Chem. Technol. Biotechnol. 90 (9), 1677–1684. https://doi.org/10.1002/jctb.4476.

Kanmani, P., Rhim, J.W., 2014. Antimicrobial and physical-mechanical properties of agar-based films incorporated with grapefruit seed extract. Carbohydr. Polym. 102, 708–716. https://doi.org/10.1016/j.carbpol.2013.10.099.

Khan, G.M.A., Terano, M., Gafur, M.A., Alam, M.S., 2016. Studies on the mechanical properties of woven jute fabric reinforced poly(L-lactic acid) composites. J. King Saud Univ. - Eng. Sci. 28 (1), 69–74. https://doi.org/10.1016/j.jksues.2013.12.002.

Mahmoudi Khatir, N., Abdul-Malek, Z., Zak, A.K., Akbari, A., Sabbagh, F., 2016. Sol–gel grown Fe-doped ZnO nanoparticles: antibacterial and structural behaviors. J. Sol-Gel Sci. Technol. 78 (1), 91–98. https://doi.org/10.1007/s10971-015-3922-y.

Lagarón, J.M., López-Rubio, A., José Fabra, M., 2016. Bio-based packaging. J. Appl. Polym. Sci. 133. https://doi.org/10.1002/app.42971.

Lavand, A.B., Malghe, Y.S., 2018. Synthesis, characterization and visible light photocatalytic activity of carbon and iron modified ZnO. J. King Saud Univ. - Sci. 30 (1), 65–74. https://doi.org/10.1016/j.jksus.2016.08.009.

Li, W., Li, L., Cao, Y., Lan, T., Chen, H., Qin, Y., 2017. Effects of PLA film incorporated with ZnO nanoparticle on the quality attributes of fresh-cut apple. Nanomaterials 7, 207. https://doi.org/10.3390/nano7080207.

Liew, W.C., Muhamad, I.I., 2019. Synergistic effect of graphene oxide and zinc oxide nanocomposite on antimicrobial activity. IPSB 2019, 9–12.

Mao, N.D., Jeong, H., Ngan Nguyen, T.K., Loan Nguyen, T.M., Vi Do, T.V., Ha Thuc, C.N., Perré, P., Ko, S.C., Kim, H.G., Tran, D.T., 2019. Polyethylene glycol functionalized graphene oxide and its influences on properties of Poly(lactic acid) biohybrid materials. Compos. Part B Eng. 161, 651–658. https://doi.org/10.1016/j.compositesb.2018.12.152.

Marques, P.A.A.P., Gonçalves, G., Singh, M.K., Grácio, J., 2012. Graphene oxide and hydroxyapatite as fillers of polylactic acid nanocomposites: preparation and characterization. J. Nanosci. Nanotechnol. 12, 6686–6692. https://doi.org/10.1166/jnn.2012.4565.

Ngo, T.M.P., Dang, T.M.Q., Tran, T.X., Rachtanapun, P., 2018. Effects of zinc oxide nanoparticles on the properties of pectin/alginate edible films. Int. J. Polym. Sci., 1–9 https://doi.org/10.1155/2018/5645797.

Panaitescu, D.M., Frone, A.N., Chiulan, I., Gabor, R.A., Spataru, I.C., Căşărică, A., 2017. Biocomposites from polylactic acid and bacterial cellulose nanofibers obtained by mechanical treatment. BioResources 12, 662–672. https://doi.org/10.15376/biores.12.1.662-672.

Pantani, R., Gorrasi, G., Vigliotta, G., Murariu, M., Dubois, P., Pantani, R., Dubois, P., Vigliotta, G., 2013. PLA-ZnO nanocomposite films: Water vapor barrier properties and specific end-use characteristics. Eur. Polym. J. 49, 3471–3482. https://doi.org/10.1016/j.eurpolymj.2013.08.005.

Park, S., Jeon, Y., Han, T., Kim, S., Gwon, Y., Kim, J., 2020. Nanoscale manufacturing as an enabling strategy for the design of smart food packaging systems. Food Packag. Shelf Life 26,. https://doi.org/10.1016/j.fpsl.2020.100570 100570.

Qu, P., Gao, Y., Wu, G.F., Zhang, L.P., 2010. Nanocomposites of Poly(lactic acid) reinforced with cellulose nanofibrils. BioResources 5, 1811–1823. https://doi.org/10.15376/biores.5.3.1811-1823.

Rajaura, R.S., Sharma, V., Ronin, R.S., Gupta, D.K., Srivastava, S., Agrawal, K., Vijay, Y. K., 2017. Synthesis, characterization and enhanced antimicrobial activity of reduced graphene oxide – zinc oxide nanocomposite. Mater. Res. Express 4 (2), 025401. https://doi.org/10.1088/2053-1591/aa5bff.

Raquez, J.-M., Habibi, Y., Murariu, M., Dubois, P., 2013. Polylactide (PLA)-based nanocomposites. Prog. Polym. Sci. 38, 1504–1542. https://doi.org/10.1016/j.progpolymsci.2013.05.014.

Rokbani, H., Daigle, F., Ajji, A., 2019. Long- and short-term antibacterial properties of low-density polyethylene-based films coated with zinc oxide nanoparticles for potential use in food packaging. J. Plast. Film Sheeting 35 (2), 117–134. https://doi.org/10.1177/8756087918822677.

Sabbagh, F., Kiarostami, K., Khatir, N.M., Rezania, S., Muhamad, I.I., Hosseini, F., 2021. Effect of zinc content on structural, functional, morphological, and thermal properties of kappa-carrageenan/NaCMC nanocomposites. Polym. Test. 93, 106922. https://doi.org/10.1016/j.polymertesting.2020.106922.

Salehudin, M.H., Muhamad, I.I., 2018. Effect of graphene oxide and cellulose nanofiber towards mechanical properties of polylactic acid based active packaging using response surface methodology. Malaysian J. Anal. Sci. 22, 984–998. https://doi.org/10.17576/mjas-2018-2206-08.

Shankar, S., Wang, L.-F.-F., Rhim, J.-W.-W., 2018. Incorporation of zinc oxide nanoparticles improved the mechanical, water vapor barrier, UV-light barrier, and antibacterial properties of PLA-based nanocomposite films. Mater. Sci. Eng. C 93, 289–298. https://doi.org/10.1016/j.msec.2018.08.002.

Sharma, G., Kumar, A., Sharma, S., Naushad, M.u., Prakash Dwivedi, R., ALOthman, Z. A., Mola, G.T., 2019. Novel development of nanoparticles to bimetallic nanoparticles and their composites: A review. J. King Saud Univ. - Sci. 31 (2), 257–269. https://doi.org/10.1016/j.jksus.2017.06.012.

Ubaidullah, M., Al-Enizi, A.M., Shaikh, S., Ghanem, M.A., Mane, R.S., 2020. Waste PET plastic derived ZnO@NMC nanocomposite via MOF-5 construction for hydrogen and oxygen evolution reactions. J. King Saud Univ. - Sci. 32 (4), 2397–2405. https://doi.org/10.1016/j.jksus.2020.03.025.

Wang, P., Tang, S., Sheng, F., Cai, J., Fei, P., Nawaz, A., Walayat, N., Javaid, A.B., Xiong, H., 2019. Crystallization, thermal stability, barrier property, and aging resistance application of multi-functionalized graphene oxide/poly(lactide)/starch nanocomposites. Int. J. Biol. Macromol. 132, 1208–1220. https://doi.org/10.1016/j.ijbiomac.2019.03.183.

Wu, S., Chen, X., Li, T., Cui, Y., Yi, M., Ge, J., Yin, G., Li, X., He, M., 2020. Improving the performance of feather keratin/polyvinyl alcohol/tris (hydroxymethyl)

aminomethane nanocomposite films by incorporating graphene oxide or graphene. Nanomaterials 10 (2), 327. https://doi.org/10.3390/nano10020327.
Xu, P.-P., Zhang, S.-M., Huang, H.-D., Xu, L., Zhong, G.-J., Li, Z.-M., 2020. Highly efficient three-dimensional gas barrier network for biodegradable nanocomposite films at extremely low loading levels of graphene oxide nanosheets. Ind. Eng. Chem. Res. 59 (13), 5818–5827. https://doi.org/10.1021/acs.iecr.9b06810.
Yong, H., Wang, X., Bai, R., Miao, Z., Zhang, X., Liu, J., 2019. Development of antioxidant and intelligent pH-sensing packaging films by incorporating purple-fleshed sweet potato extract into chitosan matrix. Food Hydrocoll. 90, 216–224. https://doi.org/10.1016/j.foodhyd.2018.12.015.
Yuan, M., Xiong, C., Jiang, L., Li, H., Yuan, M., 2018. The preparation, characterization, mechanical and antibacterial properties of GO-ZnO nanocomposites with a poly (L-lactide)-modified surface. Materials (Basel) 11 (2), 323. https://doi.org/10.3390/ma11020323.
Zhong, L., Liu, H., Samal, M., Yun, K., 2018. Synthesis of ZnO nanoparticles-decorated spindle-shaped graphene oxide for application in synergistic antibacterial activity. J. Photochem. Photobiol. B Biol. 183, 293–301. https://doi.org/10.1016/j.jphotobiol.2018.04.048.
Zhong, L., Yun, K., 2015. Graphene oxide-modified ZnO particles: Synthesis, characterization, and antibacterial properties. Int. J. Nanomed. 10, 79–92. https://doi.org/10.2147/IJN.S88319.